MODELING THE ORTHOTROPIC EXPANSION INDUCED BY ALKALI-AGGREGATE REACTION: METHODOLOGICAL REVIEW AND PRACTICAL APPLICATION

Alfonso Pappalardo Jr.[1,*], Ruy Marcelo de Oliveira Pauletti[2],
Thomas Garcia Carmona[3], Tiago Garcia Carmona[3],
Antonio Carmona Filho[3]

[1] Escola de Engenharia da Universidade Presbiteriana Mackenzie,
São Paulo, SP, BRAZIL

[2] Escola Politécnica da Universidade de São Paulo,
São Paulo, SP, BRAZIL

[3] Carmona Soluções de Engenharia
São Paulo, SP, BRAZIL

Abstract

Many concrete reinforced structures throughout the world are suffering from deterioration induced by Alkali-Aggregate Reaction (AAR), with direct impact on their durability and serviceability. AAR produces concrete expansion, generally leading to undesirable deformations throughout the structure. Several methodologies have been proposed for using collected field data to feedback predictive mathematical models, usually based on Finite Element Method (FEM) for the interpretation and prediction of the behavior of concrete exposed to AAR. In this paper, we briefly review the AAR phenomenon and some of the mathematical models used to simulate it, and propose a numerical approach to simulate the orthotropic swelling of concrete subjected to AAR, by means of conveniently adjusted orthotropic thermal expansion coefficients. The methodology, which takes into account the influence of the induced confining compressive stress state, the restraint due to steel reinforcement and the relative humidity of concrete, is then applied to model the AAR effects on the actual case of a pillar and the foundation block supporting the arches of a large steel roof structure.

Keywords: AAR, Alkali-Aggregate reaction, mathematical model, orthotropic swelling, confinement stress, reinforcement restraint

1 INTRODUCTION

1.1 Mechanism of Alkali-Silica Reaction

The AAR, especially the Alkali-Silica Reaction, is a chemical reaction between the silica minerals contained in concrete aggregates and the hydroxyl ions present in pore fluids of conventional Portland cement, which causes an irreversible anisotropic volumetric expansion. At early stages, the alkali-silica gel formed by the chemical reaction expands by water absorption, until the concrete voids are completely filled. From this point on, a significant osmotic pressure is established, which leads to internal micro cracking throughout the concrete mass. The intensity, spatial distribution and time evolution of AAR expansion process in concrete structures are influenced by many factors, such as: (i) the amount and type of reactive aggregates present; (ii) amount of alkalis from external sources; (iii) the moisture content; (iv) the concrete temperature; (v) the three-dimensional stress state; (vi) the reinforcement ratio in orthogonal directions.

On the other hand, several studies have shown that the expansion rates of the alkali-silica reaction of cement can be significantly reduced by the addition of alumina-silicate. In fact, while the type of aggregate and the amount of alkali contained in concrete may be potentially reactive and, under certain unfavorable conditions, promote AAR and deterioration of the material, it has also been observed that a new class of construction materials, the Alkali-Activated Cementitious Materials (AAC), can actually benefit from this reaction. AAC reactions comprises essentially two phases: the first corresponds to the dissolution of silica and alumina, when the starting material ('precursor') is mixed with the alkali solution ('activator') and the second, characterized by polycondensation, produces materials which rapidly harden and gain mechanical and chemical resistance, at room temperature [4]. The resulting materials are highly durable, with low

* Correspondence to: alfonso@mackenzie.br

permeability, which also increases resistance to acid attack and protects the steel reinforcement. Compared to normal Portland cement, these new materials yield a more ecologically efficient and sustainable concrete, drastically reducing greenhouse effect and embodied energy. There is abundance of raw materials in nature, and use can be made of industrial by-products as well as of mining and construction waste. Also, these materials may be mixed with silica contaminated aggregates, developing chemical links in aggregate interface that further contribute to improving mechanical properties. Cements obtained by alkaline activation can be advantageous in many industrial and engineering applications: composite materials for fire protection, resins for externally bonded fiber-reinforced composite system in reinforced concrete structures, encapsulation of heavy metals waste in mine tailing and immobilization of toxic-radioactive residual material from nuclear reactors, refractory materials industry, production of prefabricated concrete elements, soil stabilization, construction of marine and coastal structures, among others [4]. Figure 1 shows, comparatively, the reaction mechanisms for production of AAR and AAC and related advantages and disadvantages.

2 COMPUTATIONAL MECHANICS

2.1 General considerations

Numerical modelling of the AAR concrete expansion is usually performed by means of the Finite Element Method (FEM). The construction of a finite element model is necessary prior and after installation of the monitoring system to assessment of the long-term structural effects of AAR. Before installation of monitoring system, a finite element model allows: (i) explaining the anomalous behavior observed by visual inspections; (ii) guiding the type and spatial disposition of monitoring instruments. After, these models are necessary to: (iii) interpreting field data; (iv) predicting the long-term effects of AAR; (v) estimating serviceability, safety and stability of the construction under different loading scenarios; (vi) selecting efficient structural rehabilitation methods and (vii) predicting long-term corrective measures for concrete repair [5].

Generally speaking, simulation of AAR concrete swelling along the time, considering all influencing factors, requires incremental multi-step nonlinear Finite Element Analyses (FEA), and therefore also large computational resources. In the 90's, supercomputers were required to run the fully nonlinear coupled-field mathematical model (structure and foundation), such as the 300,000 degrees of freedom model shown in Figure 2 [6]. Evolution of computers and software in the last two decades now allows running nonlinear coupled-field FEA also in low cost personal computers and many commercial software packages are available, with advanced graphical interfaces and capability to model the many features involved in AAR analyses: coupled-field analysis, fracture mechanics, contact analysis, transport analysis (moisture-heat analysis, heat transfer analysis), nonlinear analysis of reinforced concrete structures and user defined subroutines for the description of nonlinear phenomena (creep and shrinkage analysis, chemical swelling, and so on). Table 1 lists general purpose commercial finite element that includes capabilities to suitable simulation of AAR expansions.

2.2 Constitutive models

The combination of modern numerical analysis techniques and high-speed digital computers provide a powerful tool for the nonlinear analysis of concrete structures. In particular, modelling reinforced concrete requires a consistent representation of the steel-concrete interface, which can be satisfactory achieved by means of adequate stress-strain constitutive laws.

2.2.1 Constitutive models for reinforced concrete

Constitutive models to represent the nonlinear behavior of concrete requires consideration of two distinct phases in the stress-strain curve, with both elastic and inelastic deformations. A proper constitutive model for analysis of concrete structures requires a complete description of the behavior of concrete in both ascending post-failure branch (strain-hardening behavior), considering the contribution of the tensile stiffness of reinforcing bars, and descending post-failure branch (strain-softening behavior). This constitutive model is used to reproduce stress-strain relations for different loading conditions, especially under compressive confining pressure. Experimental data indicate nonlinear relationships between hydrostatic pressure and the shearing capacity, with the failure surface presenting curved meridians. The standard Mohr-Coulomb criterion is insufficient to represent this effect. It was also observed experimentally that a section in deviatoric plane of concrete failure surface isn't circular, but depends on the angle of similarity. In this sense, the rupture surfaces are better described by a Willam-Warnke triaxial strength failure criterion [3]. The peak value of effective stress in compression $f'c$ and the effective stress in tension $f't$ are calculated according to this failure criterion. Above these values, crushing and cracking mechanisms are triggered.

The failure surface of concrete is generally expressed in the form $f(\rho,\sigma_m,\theta)= \rho - \rho_f =0$, where f is the failure surface, $\rho=(2J_2)^{1/2}$ is the stress component perpendicular to the hydrostatic plane, defined by the second invariant of the stress deviator tensor (J_2), σ_m is the mean stress, θ is the similarity angle and ρ_f

defines the failure envelope on the deviatoric plane according to the Willam-Warnke failure model [3]. A discrete approach is used to represent steel reinforcement. The reinforcement is in uniaxial stress state and its constitutive law is a bilinear stress-strain diagram, with the classic Mises stress criterion being adopted to analytically define the plasticity yield surfaces. A smeared approach is used to model cracks and the no bond-slip relationship was modeled directly. The complete equivalent uniaxial stress-strain diagrams for all materials, including the reinforcement steel-bond model, are shown in Figure 3.

The material properties are assumed uniform within each finite element. A bulk constitutive model considers three-dimensional orthotropic materials with thermo-mechanical coupling: $\boldsymbol{\varepsilon} = \mathbf{C} \cdot \boldsymbol{\sigma} + \boldsymbol{\alpha} \cdot \Delta T$, where $\boldsymbol{\varepsilon}=\{\varepsilon_x, \varepsilon_y, \varepsilon_z, \gamma_{xy}, \gamma_{yz}, \gamma_{zx}\}$, $\boldsymbol{\sigma}=\{\sigma_x, \sigma_y, \sigma_z, \tau_{xy}, \tau_{yz}, \tau_{zx}\}$, $\boldsymbol{\alpha}=\{\alpha_x, \alpha_y, \alpha_z, 0, 0, 0\}$ are the strain, stress and instantaneous thermal expansion vectors. The thermal shearing coefficients are zero, i.e. the shear stresses are not affected by temperature variations. The stress vector $\boldsymbol{\sigma}$ and material stiffness matrix $\mathbf{D}=\mathbf{C}^{-1}$ can be decomposed into the different material phases (concrete, reinforcement and steel plates), according to: $\boldsymbol{\sigma} = \boldsymbol{\sigma}_c + \boldsymbol{\sigma}_r + \boldsymbol{\sigma}_s$ and $\mathbf{D} = \mathbf{D}_c + \mathbf{D}_r + \mathbf{D}_s$, in order to assess the response of each material.

2.2.2 *Constitutive models for concrete affected by AAR*

The AAR expansions are strongly influenced by the three-dimensional stress state. References studies, performed by Charlwood and published in Léger [5], represent the influence of stress state on unidirectional AAR concrete expansion by

$$\dot{\varepsilon}_g = \dot{\varepsilon}_u - K \cdot \log_{10}(\sigma_i / \sigma_L) \text{ for } \sigma_L \le \sigma_i \le \sigma_U ,$$

where $\dot{\varepsilon}_g$ is the restrained expansion rate in microstrain/year, $\dot{\varepsilon}_u$ is the unrestrained expansion rate (free expansion), σ_i is the principal stress in direction *i*, σ_L is the lower stress for which $\dot{\varepsilon}_g = \dot{\varepsilon}_u$ (i.e. the stress below which the confinement has no influence on AAR expansion) and σ_U is the upper stress for which $\dot{\varepsilon}_g = 0$ (i.e. the threshold compression stress for which the AAR expansion is stopped). On the other hand, according to the failure criterion, if the effective tension stress *f'*t is reached, a process of micro-cracking and relieve of the internal gel pressure is started. This case, cracking provides space for gel migration. Accordingly, along the weaker material axis (normal to the crack plane), the AAR expansion is reduced drastically, whereas in the stronger axis (parallel to the crack plane), the AAR expansion is reduced too. This occurs because the cracks allow absorption of the gel growth, independently of the crack directions. Figure 4 shows the theoretical model used to considering the dependence of stress-state on AAR expansions. According to this methodology, the AAR expansion can be considered as an analogue to thermal expansion, with equivalent thermal expansion coefficients defined by retro-analysis dependent on the degree of internal humidity in concrete and on the stress state. Considering a unitary temperature variation $\Delta T=1^oC$ (arbitrary value for thermal analogy) and a unitary time step increment $\Delta t=1$ year, there results:

$$\dot{\varepsilon}_{g,ij} = \alpha_{ij}^{tg} \text{ where } \left| \begin{array}{l} i = x, y, z \\ j = 1,2,3,\ldots \text{(year)} \end{array} \right.$$

and a restrained growth rate is equivalent to an instantaneous orthotropic thermal expansion coefficient, which corresponds a tangent to the expansion curve, at a given temperature.

3 CASE STUDY

3.1 Description

In this section, one will briefly present the case of the repair of the concrete bases of a large steel arch, that supports the roof of a multifunctional sport arena, shown in Figure 5a. The problem highlights the main aspects related to AAR identification, complementary tests and the adopted repair technique

The degradation of support concrete structures caused by internal sulphate reaction, with Delayed Ettringite Formation (DEF) and alkali-silica reaction (ASR) produces expansive deformations, severe cracking and loss of strength, finally leading to the reduction of the structure's lifetime, and in extreme cases forcing its demolition. In Figure 5b, we note the occurrence of superficial map-cracking in a concrete pillar as the main macroscopic evidence of these degradation phenomena. Then, Figure 5c shows the extraction of samples to undergo two expansibility tests recommended by the Brazilian standard NBR 15577 [1,2]. The DEF phenomenon was identified in all specimens extracted from distinct parts of the structure. It has been found that DEF appears in concretes frequently exposed to humidity and high temperatures, mainly during summer. These ambient conditions are frequent at the construction site, where the ambient temperature frequently reaches up to 40 Celsius degrees. To avoid the demolition of the damaged support structures, it was suggested to encase the concrete pillars with steel plates bonded with epoxy resin, as shown in Figures 6a and 6b. It is believed that this technique produces an external confinement that will eventually reduce the deleterious expansions.

In order to assess the evolution of stresses in the reinforcing plates and rebars of the pillars and foundation blocks, an instrumentation system composed by electrical extensometer type strain gage was installed, as shown in Figure 6c.

3.2 Mathematical model

The finite element model is composed of a mesh of three-dimensional eight-node brick elements, two-dimensional four-node membrane-shell elements and unidimensional two-node truss elements to represent the foundation composed by reinforced concrete pillar and foundation block. All elements have a compatible translational degrees of freedom. The pile caps were not considered in the mathematical model. The materials properties used were concrete group C25 (uniaxial compressive strength fc=25 MPa, Young´s module E=23800 MPa, Poisson ratio ν=0.2 and specific weight γ=25 kN/m^3) for the pillar, concrete group C-20 (uniaxial compressive strength fc=20 MPa, Young´s module E=21287 MPa, Poisson ratio ν=0.2 and specific weight γ=25 kN/m^3) for the foundation block, and steel class CA-50 (yield strength fy=500 MPa, Young´s module E=210000 MPa, Poisson ratio ν=0.3 and specific weight γ=78.5 kN/m^3) for rebars and steel class ASTM A-570 (yield strength fy=310 MPa, Young´s module E=205000 MPa, Poisson ratio ν=0.3 and specific weight γ=78.5 kN/m^3) for reinforcing plates. The nonlinear properties for the Willan-Warnkee rupture surface are the uniaxial tensile strength f t=0.1 fc, the biaxial compressive strength f bc=1.15 fc, the confined biaxial compressive strength f 1=1.73 fc and the confined uniaxial compressive strength f 2=1.45 fc [3,6]. The dimensions of a pillar are 3.44 meters in diameter and 3.90 meters in height, and block dimensions are 6.20 meters (width) x 6.20 meters (depth) x 2.10 meters (height). Steel bars of 8 mm, 12.5 mm and 20 mm (effective diameter) were used for reinforcement. The thickness of reinforcing plates is 5 mm.

The model's boundary conditions are: all degree of freedom restrained at the block-soil interface, to neglect soil-structure interaction; symmetry boundary conditions at the symmetry plane prescribed displacement in the pillar to represent the action and the confinement due to the roof steel structure, as illustrated in Figure 8.

To consider the influence of the humidity and the temperature, according observed in samples extracted from the structure, the pillar was divided into one outside region where there was a high moisture content and a drier internal region. The initial conditions assumed for AAR free-expansion rate was 135 με/year and 60 με/year for the outer part of the pillar, and for its core part and foundation block, respectively. These values were obtained from published data and adapted to data gathered from expansibility tests [6], as shown in Figure 7. In FEA, we have neglected the long-term effects due creep as well as the decrease of AAR expansion rate over time, because the observation period was less than three years. To simulate the shrinkage a 300με uniform deformation was imposed as initial conditions of the problem. The Willam-Warnke rupture surface was used only for calculating the effective tension stress f't to relief of stress induced by AAR expansions, shown in Figure 7. We also assumed that the interfaces steel-concrete are perfectly bonded, both the bars and for reinforcing plates. Birth and death resouces was used to simulate the installation of the strengthening system after the initial process of concrete AAR expansions.

For incremental solutions, we consider three time-steps: the first time step was used to impose the initial conditions of the problem, the second one to simulate one year after AAR identification and installations of strengthening system and the third one to simulate one year after the repair work. Orthotropic tangent thermal expansion coefficients equivalent to the restrained expansion rate for one year were used for the whole incremental solution.

4 RESULTS

Figure 9 shows axial stresses in rebars, one year after AAR identification. Figures 10 and 11 show vertical AAR expansions on block and pillar for one year after AAR identification and one year after installation of strengthening system. Figure 12 indicate the minimum principal stress σ_3 distributions on the external layer of concrete pillar for one year after AAR identification and one year after installation of the system strengthening. Figure 13 shows Mises stresses on reinforcing plates one year after installation of system strengthening. Finally, the Figure 14 displays the evolution of vertical AAR expansions in the period between the construction and one year after repair.

5 DISCUSSION

In Figure 9 we notice an increase in tensions in the stirrups of the column due to the expansive reaction. From the analysis of Figure 10, we also notice that the expansions by AAR are still ongoing in the foundation block. It is also observed in Figure 11 that the confinement produced by the reinforcement plate mitigated the vertical expansions at the pillar's lateral surface. Moreover, the vertical expansion continues, reaching twice the value at the top of the pillar, with respect to the values observed at the lateral surface, producing considerable bending of the reinforcing plate.

Figure 12 shows the minimum principal stresses σ_3, which are effectively stabilized by the confinement still produced by the reinforcement plate. Figure 13 shows the numerical and experimental data of increased in Von Mises stresses in the reinforcement plate, one year after the installation, and the tendency of these stresses to stabilize as an effect of the confinement. Despite the short observation period of the instrumentation data, it was experimentally observed that the deformation of the strain gage plate installed at point S2 (magenta curve in Figure 13b) corresponds to a extrapolate stress value of 90 MPa after about one year of readings. This result corroborates those obtained in the numerical analyses. Finally, Figure 14 shows the evolution of the expansion due to AAR, confirming the effectiveness of the reinforcement system to control of the deformations produced by the AAR.

Further research may consider extensive expansibility tests on cracked specimens, to quantify the AAR expansions in directions parallel and perpendicular to the cracking plane. We also propose in mathematical model the consideration of AAR orthotropic thermal expansions oriented in principal strain directions.

6 CONCLUSIONS

Generally speaking, in a coupled-field analysis the temperature and moisture transport and nonlinear static analyses should be performed simultaneously. However, as moisture and temperature distributions does not depend significantly on structural deformations, it is suggested that uncoupling the problem and performing a staggered solution still yields accurate results. The moisture transport, leading to moisture gradients inside the structure, has not been considered in this work. In the near future, full coupled-field analysis will be performed in powerful personal computers and workstations, to assess this working hypothesis.

The proposed nonlinear mathematical models allowed to clearly describe the failure mechanisms of structural elements affected by AAR in the selected case study. The numerical results showed satisfactory correlation with the experimental results, which by their turn highlighted the importance of calibration of mathematical model and validation according to field data.

From its first developments, in the 60's, the FEM has become the most effective method to solve problems in continuous mechanics, and remains the dominant method today. Improved iterative solvers, meshless formulations, special-purpose elements, adequate theory of failure for innovative materials, design process with optimization tools are on the list of things to improve structural modelling via FEM in the near future. Particularly in the case of AAR modeling, adequate mechanical and chemical properties of the materials affected by AAR are difficult to acquire, fatigue data is often lacking, AAR expansions due multiaxial stress state involves insightful construction of prototypes and their exhaustive testing. These are some of the challenges to be tackled by AAR researches in the coming decades.

7 REFERENCES

[1] Associação Brasileira de Normas Técnicas NBR 15577-4 (2008): Agregados - Reatividade álcali-agregado. Parte 4: Determinação da expansão em barras de argamassa pelo método acelerado. Versão Corrigida 2:2009. Rio de Janeiro, ABNT, 2008.

[2] Associação Brasileira de Normas Técnicas. NBR 15577-6 (2008): Agregados - Reatividade álcali-agregado. Parte 6: Determinação da expansão em prismas de concreto. Versão Corrigida 1:2008. Rio de Janeiro, ABNT, 2008.

[3] Chen, WF and Han, DJ (1988): Plasticity for Structural Engineers. Springer-Verlag, New York: pp 606.

[4] Davidovits, J (2009): Geopolymer: Chemistry and Applications. 3. ed. Geopolymer Institute. Saint Quentin.

[5] Léger, P; Tinawi, R and Mounzer, N (1995): Numerical Simulation of Concrete Expansion in Concrete Dams Affected by Alkali-Aggregate Reaction:State-of-the-Art. Canadian Journal of Civil Eng., v.22, n.4, p.692-713.

[6] Pappalardo Jr., A (1999): Uma Metodologia para a Modelagem Matemática de Barragens de Concreto Afetadas pela RAA. 181 p. Tese (Doutorado em Engenharia Civil). Escola Politécnica da Universidade de São Paulo, São Paulo.

TABLE 1: List of top ten general purpose commercial finite element softwares.

SOFTWARE PACKAGES	MULTIPHYSICS	TRANSPORT ANALYSIS	NONLIN. RC STRUCTURES	CREEP AND SHRINKAGE	FRACTURE MECHANICS	THERMAL-STRUCTURAL	USER DEFINED SUBROUT.	DEVELOPER (COUNTRY)
ABAQUS	X	X	X			X	X	Dassault Systemes (France)
ADINA	X	X	X	X		X	X	ADINA R&D, Inc (Massashussets, USA)
ANSYS	X	X	X	X	X	X	X	ANSYS, Inc. (Pittsburgh, USA)
ATENA	X	X	X	X	X	X	X	Cervenka Consulting (Prague, Czech Republic)
COMSOL	X	X	X	X	X	X	X	COMSOL Group (Stockholm, Sweden)
DIANA		X	X	X	X	X	X	TNO DIANA BV (Delft, Netherlands)
GTSTRUDL	X	X	X	X	X	X	X	INTEGRAPH System (USA)
LUSAS		X	X	X		X		UK Software (London, United Kingdom)
NASTRAN	X	X	X	X	X	X	X	MacNeal-Schwendler Corporation (USA)
SAP2000				X		X	X	CSI Computers and Structures Inc. (USA)

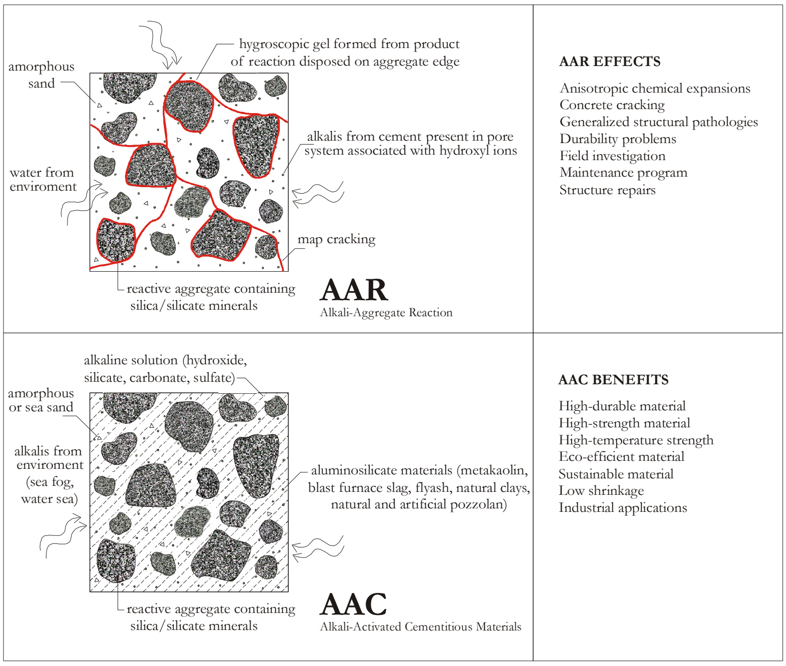

FIGURE 1: Comparison between AAR and AAC.

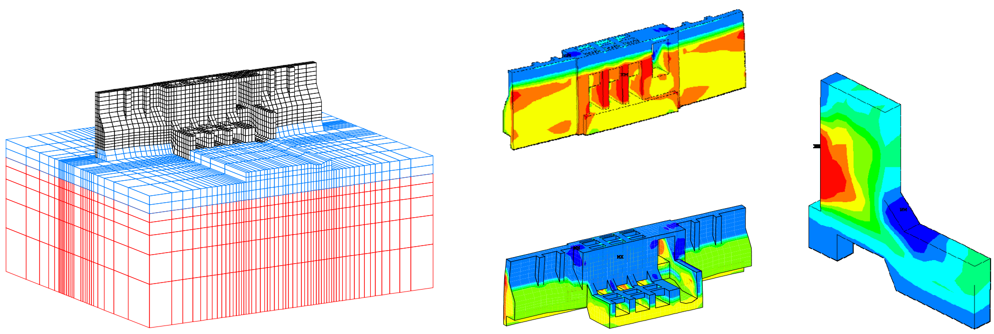

FIGURE 2: Finite element model for the analysis of Billings-Pedras Dam and associated AAR deformations after 60 years [PAPPALARDO JR., 1999].

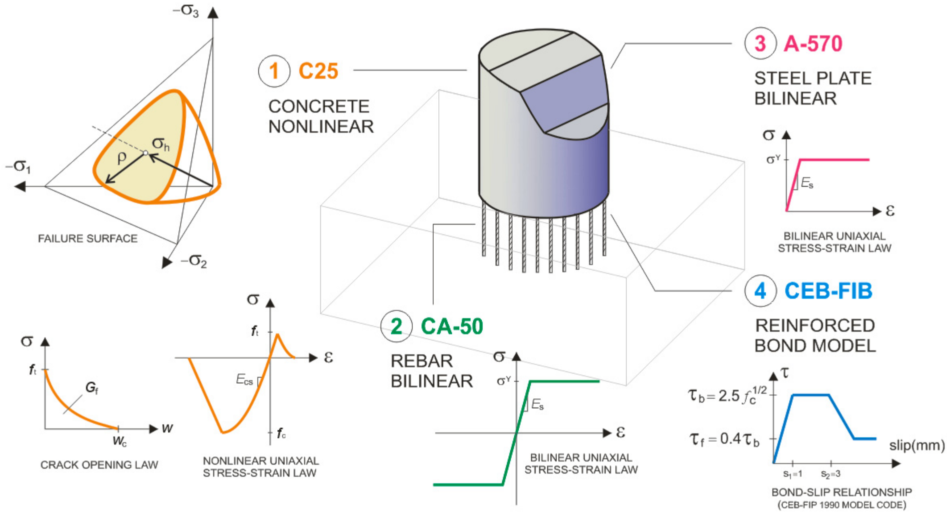

FIGURE 3: Definitions and characterization of the materials considered in the mathematical model.

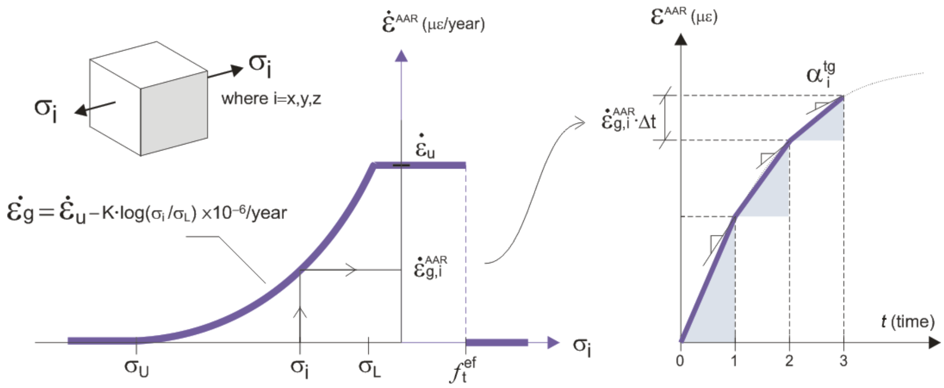

FIGURE 4: Methodology for incremental multi-step analysis.

FIGURE 5: (a) View of one of the four concrete supports of the steel roof structure affected by AAR (b) Mapped-cracks typical of AAR expansions (c) Extraction of sample for expansibility test method.

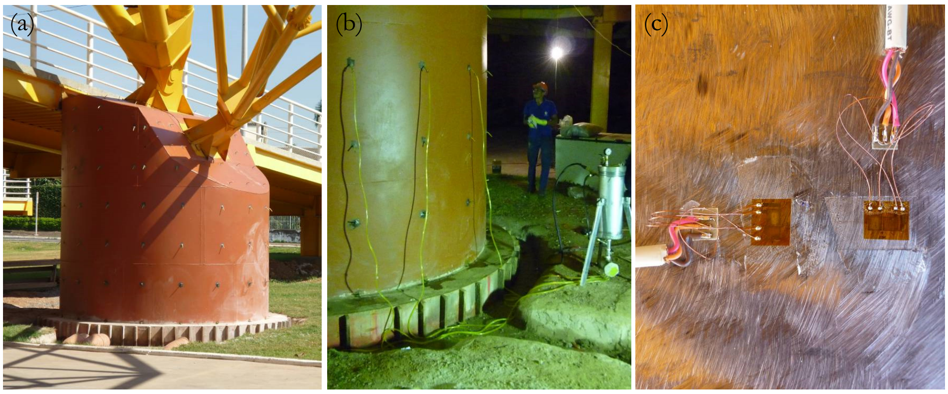

FIGURE 6: (a) Strengthening method steel-jacketed concrete pillar (b) Injection system with epoxy resin (c) Electrical extensometer type strain gage installed under the reinforcing steel plate.

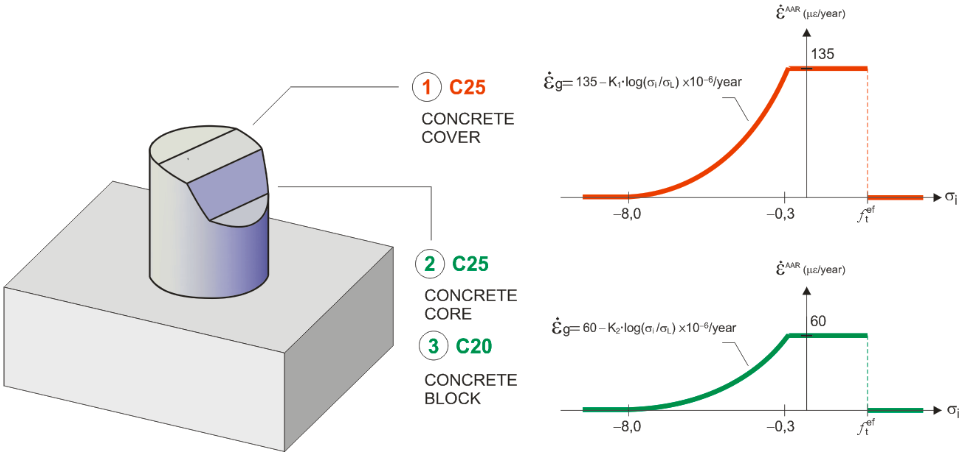

FIGURE 7: AAR Expansion Model used in set composed by pillar and block.

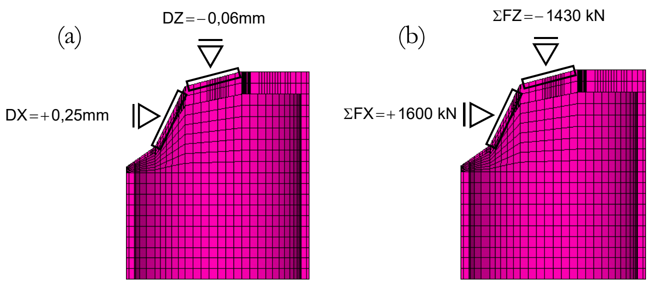

FIGURE 8: Prescribed displacements adjusted to represent steel roof action.

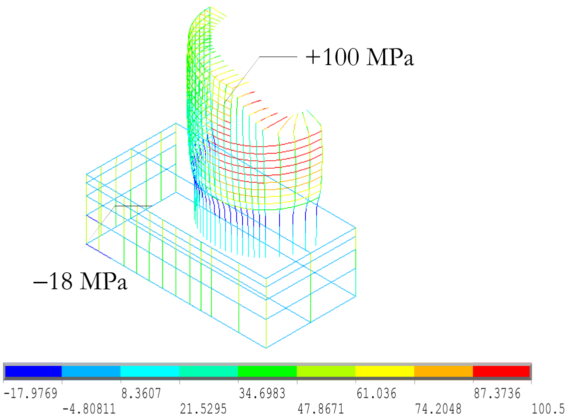

FIGURE 9: Axial stress in rebars one year after AAR identification.

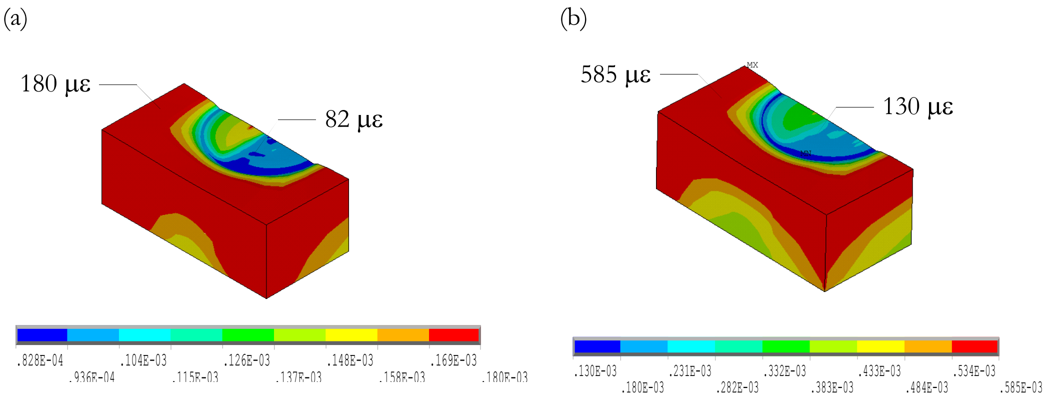

FIGURE 10: AAR vertical expansion on block (a) one year after AAR identification (b) one year after installation of strengthening system.

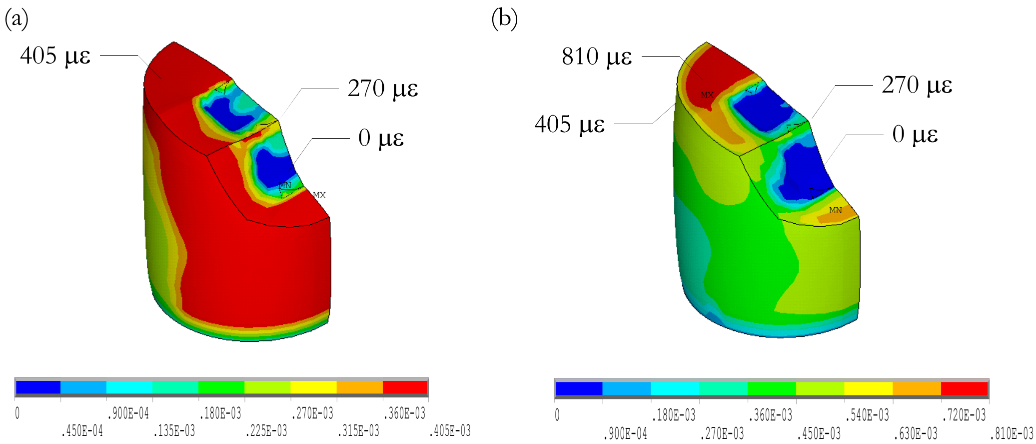

FIGURE 11: AAR vertical expansion on pillar (a) one year after AAR identification (b) one year after installation of strengthening system.

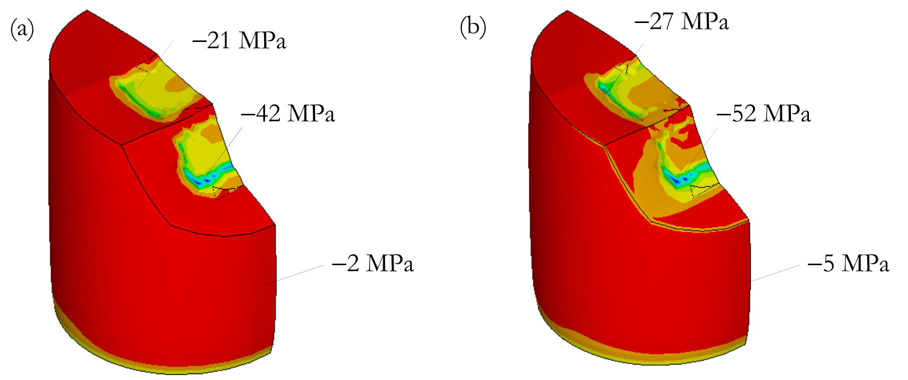

FIGURE 12: Minimum principal stress σ_3 on external layer of concrete pillar (a) one year after AAR identification (b) one year after installation of system strengthening.

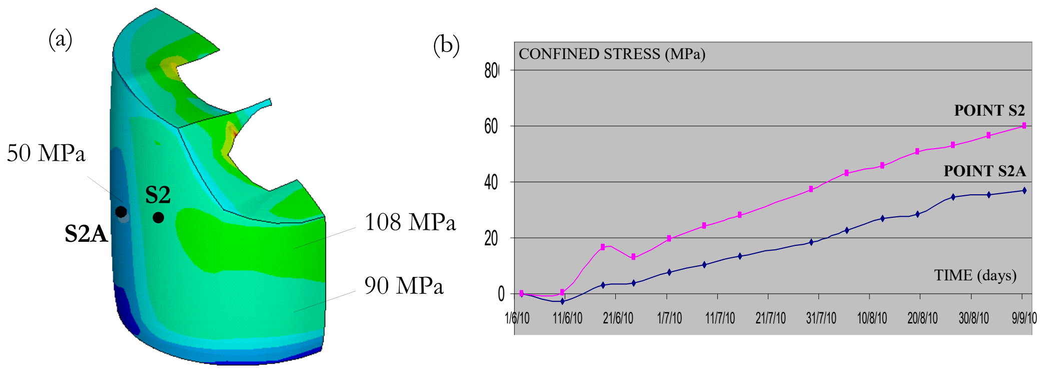

FIGURE 13: Von Mises stress on reinforcing plates one year after installation of system strengthening (a) membrane-shell element solution (b) experimental data 3 months.

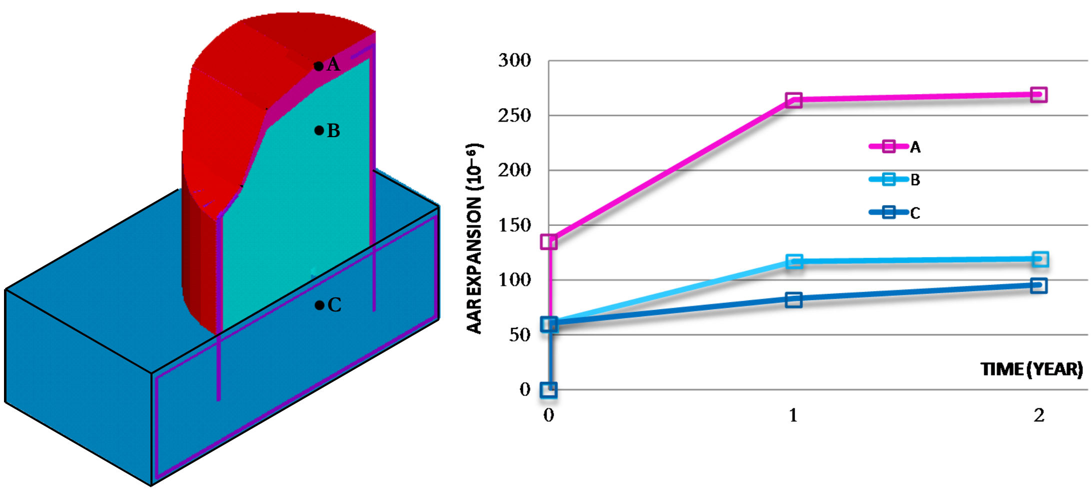

FIGURE 14: Evolution of AAR vertical expansions in the period between the construction and one year after repair.